Composite of Aromatic Polythiourea/$BaTiO_3$ Nanowires with High Energy Density and High Discharge Efficiency for Energy Storage Applications

Li Xiali
UESTC: University of Electronic Science and Technology of China
Liuwei Shi
UESTC: University of Electronic Science and Technology of China
Lei Chen
Sichuan YongXing Electronics Co.Ltd
Wenyao Yang
Chongqing Engineering Research Center of New Energy Storage Devices and Applications
Xiaoting Zha
UESTC: University of Electronic Science and Technology of China
Chengpeng Wang
UESTC: University of Electronic Science and Technology of China
Runhui Xi
UESTC: University of Electronic Science and Technology of China
Jianhua Xu
UESTC: University of Electronic Science and Technology of China
Yajie Yang (jj_eagle@163.com)
UESTC: University of Electronic Science and Technology of China https://orcid.org/0000-0002-5292-0349

Research Article

Keywords: Aromatic polythiourea (ArPTU), BaTiO3 (BT), Dopamine (Dopa),HDMLP

Posted Date: February 9th, 2021

DOI: https://doi.org/10.21203/rs.3.rs-162596/v1

Version of Record: A version of this preprint was published at Journal of Materials Science: Materials in Electronics on July 6th, 2021. See the published version at https://doi.org/10.1007/s10854-021-06450-z.

Abstract

Ceramic/polymer nanocomposites have shown great potential in high energy storage density capacitors for pulsed power applications. However, due to the difference in surface energy between inorganic fillers and polymers, the discharge energy density and efficiency of nanocomposites are limited. In this article, the $BaTiO_3$ (BT) nanowires (nws) modified with dopamine (Dopa) was introduced into aromatic polythiourea (ArPTU) polymer matrix as composite for high performance dielectrics. This is a new path about the introduction of a high dielectric constant ceramic into high dipole moment linear polymers (HDMLP), which produces the polymer composite with high energy storage density and high discharge efficiency. The composite ArPTU/BT nws shows an energy density of 7.5 J/cm^{-3} and high efficiency more than 90 % is obtained under an electric field of 250 MV/m^{-1}. It also has been found that the modification of BT nws with the dopamine reduces the dielectric loss of composite effectively due to the good synergistic effective between ArPTU and BT nws, and high stability of composite for energy storage is also achieved. This work provides an effective solution for achieving high energy storage density and high discharge efficiency in polymer dielectrics for practical capacitor applications.

1. Introduction

Film capacitors have the advantages of high insulation resistance, low dielectric loss and high power density. They have been widely used in mobile phones, computers, home appliances and power system, etc [1]. Dielectric film materials is the key material for film capacitors, which allows the revolution of film capacitor with improved performance. At present, the dielectric film materials for film capacitors are mainly biaxially oriented polypropylene (BOPP) [2].The breakdown strength of BOPP can reach 600 MV/m^{-1}, and the dielectric loss is only 0.0002. However, the dielectric constant of BOPP is only 2.2 (at 1 *kHz*), resulting in an energy density lower than 2.5 J/cm^{-3}.Therefore, the development of dielectric materials significantly improves the energy density of electrostatic capacitors for new technologies are imperative.

In the past decade, the ferroelectric polymers, such as polyvinylidene fluoride (PVDF), have been widely used in electrical energy storage capacitors due to its high dipole moment. However, PVDF has a very high dipole correlation through dipole coupling, causing high ferroelectric loss. For linear dielectrics, the energy storage density is calculated according to the equation $U = \frac{\varepsilon_r \varepsilon_0 E_b^2}{2}$, where ε_r is the relative permittivity, ε_0 is the vacuum permittivity, and E_b is the breakdown strength. Polymers generally have high E_b but very small ε_r. Most linear polymer dielectrics are non-polar or weakly polar, which results in linear dielectric polymers with low dipole moment and low dipole density [3]. Recently, compared with widely used non-polar or weak dipole polymers, linear polymer dielectrics with polar groups (HDMLP) has attracted great attention due to they can achieve a relatively high dielectric constant owing to high dipole moment in molecular structures. Polyureas, Aliphatic Polythioureas and Aromatic Polythiourea (ArPTU) are the most common high dipole moment linear polymers (HDMLP). Among these HDMLP, the higher

electronegativity of sulfur in the thiourea unit results in higher coupling strength of the Polythiourea. In particular, ArPTU contains high dipole moment, low dielectric loss, tunable molecular structure and amorphous glass phase structure, which make it suitable for high performance polymer dielectrics for capacitor applications. It has been found that the large dipole moment of the thiourea functional group can form the scattering centers and traps of charge carriers, thereby further reducing the conduction loss. Due to the amorphous phase structure, the dipole coupling in ArPTU is very weak, and there is no polarization hysteresis even under high electric fields, which results in high energy storage efficiency of dielectrics [3-5].

Ferroelectric ceramics have a dielectric constant of hundreds or even thousands due to spontaneous polarization. As a common ferroelectric material, $BaTiO_3$ (BT) has a relatively high dielectric constant [1]. Although HDMLP have higher breakdown electric field, their dielectric constant is much smaller than that of ferroelectric ceramic materials. So, the combination of these polymers with Ferroelectric ceramics will produce high performance composite dielectrics with high energy storage density and efficiency. Furthermore, according to the reported works, there is still lack of researches on constructing high performance polymer dielectrics based on HDMLP and Ferroelectric ceramics nanostructures. In this paper, high dielectric constant ceramic nanomaterials was introduced into ArPTU matrix for high energy storage density and discharge efficiency. In the ceramic/HDMLP composite, the dielectric properties depend on the size, concentration, and shape of the high-dielectric filler. Compared with spherical nano-sized fillers, one-dimensional(1D) nanowires show higher energy storage characteristics in dielectric and energy storage applications due to their high aspect ratio [6,7]. However, if a ceramic material with a high dielectric constant is directly added to the polymer, due to a large electrical mismatch, the electric field distribution of the entire composite material is uneven, and the breakdown strength of the composite film is greatly reduced. Therefore, an interface modification method was adopted to improve interface compatibility and adjust local interface electrical and dielectric behavior. Common organic modifiers include dopamine (Dopa) and phosphoric acid were used in this paper. These modifiers can be physically adsorbed on the filler surface through electrostatic interaction or hydrogen bonding which can also make sure good synergistic effect between nanofillers and matrix. Surface modified BT nanowires (nws) (Dopa@BT) was mixed with ArPTU polymer and a solution casting method was used to prepare Dopa@BT/ArPTU composite films with large film area. Experimental results show that when 3 *wt.%* Dopa@BT is incorporated, dielectric constant of composite is two orders of magnitude than that of pure ArPTU, and its breakdown voltage remains at a relatively high level, and the overall energy density is increased accordingly.

2. Experimental Part

2.1 Materials

Nano titanium dioxide (TiO_2), sodium hydroxide (NaOH) and barium hydroxide (octahydrate) ($Ba(OH)_2$ $8H_2O$) were purchased from Sigma and used with received. The mass molecule number of TiO_2 is 198.27 *MW* and its particle size is 5-10 *nm*. The molecular weight of NaOH is 40 *MW*. The molecular weight of

$Ba(OH)_2\ 8H_2O$ is 315.46 *MW*.4,4'diphenylmethanediamine (MDA) was purchased from Aladdin (Shanghai, China) with mass molecule number of 198.27 *MW*. p-Phenylenediisothiocyanate(PDTC) was purchased from Acros (Belgium). Its mass molecule number is 192.27 *MW*. Nmethylpyrrolidone (NMP) was supplied by Chengdu Kelong Chemical Company.

2.2 Synthesis of ArPTU

The ArPTU synthesis process utilizes the polycondensation reaction of MDA and PDTC in NMP solution [8-11].First, 20 *ml* of NMP solution was introduced into a sample bottle. Then, 0.005 *mol* of MDA was introduced into the NMP solution. After the MDA was completely dissolved, 0.005 *mol* of PDTC was added into the mixed solution. At same time, nitrogen was introduced and the mixed solution was magnetically stirred for 6 hours. After the stirring was completed, methanol was used to precipitate the product and ultrasonically cleaned at least 5 times. Finally, the obtained white solid was dried at a temperature of 60 °C for 12 hours and the obtained white fibrous solid was polythiourea.

Scheme 1 is the synthesis reaction of polythiourea. From the formula, it can be seen that due to the existence of bipolar thiourea monomer ($H_4N_2C=S$) as an inherent dipole moment, which makes its dielectric constant much larger than other linear dielectric materials. The amino group of MDA and the isothiocyanate group of PDTC polymerize to form a disubstituted thiourea group (-NH-(C=S)-NH-).It can be seen from the chemical formula of ArPTU that the dipole group is connected to the main chain, and the increase of the dielectric constant is limited due to the difficulty of the main chain to rotate.

2.3 Preparation process of BT nws

BT nws are synthesized by a two-step hydrothermal method [12-16]. In the first step, 3 *g* of titanium dioxide powder was added to the 10 $mol·L^{-1}$ NaOH solution and stirred vigorously for 2 hours. Then the obtained solution was put in a vacuum drying oven at 200 °C for 72 hours. Next, the resultant product was washed with deionized water until PH=7. And the washed product was dried in a freeze dryer for 12 hours. Finally, white $Na_2Ti_3O_7$ powder was obtained. In the second step, 0.6 *g* of the dried $Na_2Ti_3O_7$ powder was slowly added to the 0.1 $mol·L^{-1}$ $Ba(OH)_2$ solution, and stirred vigorously for 2 hours. Then the obtained solution was put it in a vacuum drying oven at 95 °C for 24 hours. The final product was filtered and cleaned with deionized water and ethanol, then cleaned product was dried in a freeze dryer for 12 hours to obtain white BT nws powder [17,18].

2.4 Modification of BT nws

Before the preparation of nanocomposites, nanowires need to be modified to reduce their surface energy and improve the dispersion ability in polymer matrix. Accordingly, nanowires was treated in modifier of Dopa for surface modification. Dopa molecule contains a large number of catechol functional groups. Under aerobic and humid weak alkaline conditions, Dopa will undergo oxidative self-polymerization to generate a series of oligomers with different molecular weights. Part of these oligomers undergoes cross-linking reactions to produce polymers with higher molecular weights. Scheme 2 is the cross-linking

reaction formula of Dopa. In the solution, Dopa has strong adhesion and can adhere to the surface of BT to functionalize the surface. Dopa is extremely sensitive to PH. It self-polymerizes and adheres to the surface of the material when it is weakly alkaline. In this process, the pH value of the solution must be controlled. In addition, the role of oxygen in the reaction process is very important.

In the process of dopamine coating on BT nws, at first, 0.6 *g* BT nws was added in a buffer solution with a dopamine concentration of 2 $g·L^{-1}$. Next, pH of the solution was adjusted to 8.5 with ammonia. Subsequently, the solution was stirred for 12 hours in a water bath at a temperature of 60 °C. After that, the products after the water bath were washed with alcohol and deionized water respectively. Finally, the product was put into a freeze dryer and freeze-dried for 12 hours to obtain Dopa@BT nws powder.

2.5 Preparation of composite film

Firstly, the Dopa@BT nws was thoroughly dispersed in the NMP solution by ultrasonic treatment for 1 hour. Subsequently, a certain amount of ArPTU was added into Dopa@BT nws solution and stirred vigorously for 12 hours. Then, the mixed solution was cast onto a glass plate with a doctor blade, and then heated at 60 °C for 12 hours to evaporate NMP. The typical thickness of these nanocomposite film is about 10 μm. For comparison, the Dopa@BT nws/ArPTU with different mass fractions (1 *wt.%*, 3 *wt.%*, 5 *wt.%*, 7 *wt.%* and 10 *wt.%*) were prepared. The preparation process of dielectric composite film is shown in Fig. 1.

3. Characterization

Scanning electron microscopy (SEM, Hitachi S-4800) and transmission electron microscopy (TEM) were used to characterize the morphology of inorganic nanoparticles and dielectric polymer films. Fourier transform infrared spectrum (FTIR) (characterized by Japan's Shimada Hikari 8400S spectrometer) was used to observe the spectrum curve of the dielectric polymer film. X-ray diffraction (XRD) was characterized to analyze the diffraction peaks and positions of dielectric polymer films. The contact angles of the nanoparticles were measured using an optical contact Angle meter (Biolin's Theta Flex) to determine the effect of dopamine modification on their dispersion. Breakdown strength of the dielectric polymer film was tested with an AC and DC withstand voltage insulation resistance tester (TH9201) at room temperature. An impedance analyzer (Agilent 4294A) was used to measure the dielectric properties in the frequency range of 100 *Hz* to 1 *MHz*. A ferroelectric test system tester (Precision Premier II) with a high-voltage power supply was used to obtain the displacement electric field circuit (D-E) in silicon oil at a frequency of 100 *Hz* at room temperature. The efficiency of the charge and discharge cycle is a function of the electric field and depends on the discharge energy and the stored energy. Co-simulation of dielectric polymer films was performed using Comsol and Matlab softwares.

4. Results And Discussion

4.1 Characterization of BT nws and Dopa@BT nws

4.1.1 Morphology analysis of BT nws and Dopa@BT nws

The morphology of nanowires is closely related to the reaction temperature, time and concentration. Generally, the higher the reaction temperature, the greater the concentration of reactants and the longer the reaction time results in the larger diameter of the nanowire.

Fig. 2 shows microtopography of nanowires. It can be seen from Fig. 2(a) that a large number of uniform BT nanowire are formed, and the average length of these 1D BT nanostructures is greater than 5 microns. Combined with the local high-resolution SEM image, it can be seen that the maximum diameter of the nanowires is less than 200 nm, and it is conservatively estimated that the aspect ratio of the BT nws is above 30.Moreover, the element mapping of BT nws (Fig. 2(b), 2c) shows that the ratio of Ba and Ti is 1:1. To sum up, BT nws was effectively synthesized by two-step hydrothermal reaction.

Furthermore, the characteristics and morphological of the Dopa@BT nws were also determined by high-resolution TEM. Dopa is used as a surface modifier to improve the compatibility between BT nws filler and ArPTU matrix. Dopa can be deposited on nanowires with the evidence that a distinct thin layer is formed on the surface of BT nws. As shown in Fig. 3(a), which helps to disperse the nanowires well in the polymer matrix. It also can be seen from the Fig. 3(a), the diameter of a single BT nws is about 120 nm, and the smooth surface of the nanowire is formed. After the surface modification of Dopa, a uniformly amorphous layer of several nanometers thick can be clearly observed on the surface of the nanowire, indicating the successful modification of Dopa on BT nws. In addition, the element mapping of the Dopa@BT nws (Fig. 3(b), 3c) proved the content, coexistence of C and N elements in the ternary Dopa@BT nws .

4.1.2 Contact angle analysis of BT nws

It is well known that, surface contact angle shows great relation to the surface energy of the materials, the greater the surface energy, the smaller the contact angle with water would be presented. In order to further confirm the successful modification of the BT nws with Dopa, a surface contact angle test was characterized as shown in Fig. 4.

It can be seen from the Fig. 4 that the contact angle of BT nws and dopamine-modified BT nws is less than 90°. This phenomenon indicates that both nws are hydrophilic. The surface contact angle of pure BT nws is about 63°, indicating a relatively hydrophobic surface. However, the surface contact angle of modified BT nws is about 22°, which is more hydrophilic than unmodified BT nws. This result indicates that the C-N bonds modification of dopamine improves the hydrophilicity of the BT nws surface. The surface modification, on the one hand, changes the surface energy of BT nws and results in well dispersion of nws in polymer matrix accordingly. More importantly, it also constructs ultrathin layer to enhance synergistic effect between the BT nws and ArPTU polymer matrix.

4.2 Characterization of Dopa@BT nws/ArPTU composite film

4.2.1 SEM images of composite film

Fig. 5 shows the surface SEM images of pure ArPTU (Fig. 5(a)), 10 *wt.%* BT nws composite film (Fig. 5(b)) and 10 *wt.%* dopamine modified BT nws composite film(Fig. 5(c)). It can be seen from the figure, after the incorporation of the unmodified nanowires into ArPTU, the composite film shows a morphology with pinholes distributed in films. The reason for this phenomenon may be the incompatibility between ArPTU and BT nws [19,20]. However, the Dopa surface-modified BT nws is uniformly dispersed in the ArPTU matrix to form a uniform and high-quality nanocomposite film. The addition of dopamine effectively improves the compatibility of ArPTU and BT nws.

In addition, Fig.5 shows the cross-section SEM images of composite films (Fig. 5(d)). It can be seen from Fig. 5(d) that the BT nws with Dopa modification was well distributed inside the polymer matrix and the nanowires are tightly fixed in the matrix, indicating that the polydopamine-coated nanowires exhibit excellent compatibility with the ArPTU matrix.

4.2.2 FTIR spectrum of composite film

In order to confirm the modification of Dopa on BT nws, the FTIR analysis was performed on the nws before and after modification, as shown in Fig. 6(a). From the infrared spectrum, the new absorption peaks at 1445 cm^{-1}, 1288 cm^{-1} and 3758 cm^{-1} rising from Dopa@BT nws are observed. They correspond to the C-C skeleton vibration of the aromatic ring, the stretching vibration of the C-N bond of the aromatic amine, the stretching vibration absorption peaks of the O-H and N-H bonds respectively [20]. This spectrum further confirms the successful modification of Dopa on the BT nws. The FTIR spectrum of Dopa@BT nws/ArPTU-based nanocomposite film with given weight fraction of nws (1 *wt.%*, 3 *wt.%*, 5 *wt.%*, 7 *wt.%* and 10 *wt.%*) were also characterized, which are shown in Fig. 6(b). The peak positions of pure ArPTU and dopa@BT nws filled composite film with different volume fractions are all at the same position. With the continuous increase of BT nws quantity, the intensity of some peaks in the range of 500 cm^{-1}-1500 cm^{-1} change. This result also confirms that the inorganic ceramic BT nanowires were successfully incorporated with ArPTU.

4.2.3 XRD analysis of composite film

In order to study the crystal structure of the composite material, the XRD spectra of BT nws, Dopa@BT nws and the composite films with different mass fractions were characterized, as shown in Fig. 7. The synthesized BT nws was a perovskite structure with the evidence that the appearance of (100), (110), (111), (200), (210), (211), (220) crystal peaks and its crystal structure shows no change after the addition of Dopa (As shown in the Fig. 7(a)). In Fig. 7(b), the pure ArPTU shows no obvious characteristic peaks, indicating that the amorphous structure of ArPTU. After the addition of Dopa@BT nws, the composite film gradually transformed from an amorphous structure to a crystalline structure partly. Moreover, the intensity of the diffraction peak increases with the increase of Dopa@BT nanowire content, which means that the crystallinity of the composite film increases with the increase of Dopa@BT nanowire content [21,22].

4.3 Energy storage characteristics of composite films

4.3.1 Dielectric properties of composite films

Compared with the 0 D nanofiller, the 1 D nanofiller has a larger dipole moment, which can increase the dielectric constant of the nanocomposite at a relatively low concentration of the nanofiller. In addition, the 1 D ceramic filler has a small specific surface area, resulting in minimal agglomeration inside the polymer matrix. It can be seen from Fig. 8(a) that, with the weight fraction of BT nws increases, the effective dielectric constant of the nanocomposite can be tuned effectively. When the content of Dopa@BT nws is 10 *wt.%*, the maximum dielectric constant of the nanocomposite is about 10.6 at 1 *kHz*. The increase in the dielectric constant of the nanocomposite is due to the electric field enhancement caused by the high-*k* nanowire in the polymer matrix [23,24]. The introduction of nanowires also causes the accumulation of charge carriers at the interface of the heterogeneous system, resulting in interface polarization for improved dielectric constant. From the Fig. 8(a) , we also find that with the frequency increasing in the range of 1 *kHz* - 5 *MHz*, the dielectric constant of the polymer matrix and nanocomposite materials gradually decreases. This behavior can be attributed to the limited dipole mobility of the polymer matrix and the reduction of interface polarization at high frequencies. The interface polarization increases with the increase of the nanowire/polymer interface area, resulting in a strong frequency-dependent dielectric constant in the nanocomposite with a high load of nanowires.

For the modified BT nanowire composite film, the loss tangent values of different films show small changes, and are close to 0.03 at 1 *kHz* (Fig. 8(b)). The polar group in dopamine promotes a stronger dipole interaction with the ArPTU matrix, thereby reducing interface polarization and increasing dispersion of nanowires. We also conclude that the Dopa modifier acts as a charge trap, reducing space charge polarization and minimizing conduction paths in the polymer film, which results in reduced dielectric loss especially rising form electrical conducting. In addition, the dopamine-modified nanowires show good interface compatibility with the polymer matrix, reducing the existence of voids in composite [25,26]. With the increase of filler loading, the loss tangent increase from 0.02 to 0.035. This is attributed to the presence of free residual substances in the composite caused by the physically adsorbed organic modifier, which leads to an increase in leakage current and an increase in dielectric loss.

4.3.2 Electrical breakdown of composite materials

The breakdown strength of the composite film is a key parameter for dielectric materials especial for device applications. Moreover, in this composite films, the breakdown strength largely depends on the dielectric constant of the single filler and the polymer matrix.

$$E_f = E_0[\varphi_m\left(\frac{\varepsilon_f}{\varepsilon_m} - 1\right) + 1]^{-1} \qquad \text{(Eq.1)}$$

$$E_m = E_0[\varphi_m\left(1 - \frac{\varepsilon_m}{\varepsilon_f}\right) + \frac{\varepsilon_m}{\varepsilon_f}]^{-1} \qquad \text{(Eq.2)}$$

The Eq. 1 and Eq. 2 are the expression of the electric field in the filler and the polymer matrix. In these equation, φ_m is the volume fraction of the filler, ε_m and ε_f are the dielectric constants of the polymer

matrix and the nanofiller respectively, and E_f, E_m are the internal electric field of the polymer matrix and the nanofiller respectively. The large difference between the dielectric constants will cause extremely distortion of electric field distribution inside the entire film.

Furthermore, a finite element simulation was utilized to simulate the local electric field concentration of nanocomposites with high dielectric constant. As shown in the Fig. 9, consider the electric field distribution of BT nanoparticles and nanowires filled with the same mass fraction, it can be shown that when nanoparticles are added to the polymers, there is an electric field around the nanoparticles, which causes the distortion of internal electric field. For composite films, the breakdown phase tends to grow at the nanofiller/matrix interface, and then penetrate the particles near the breakdown path. However, when breakdown encounters in composite containing nanofiber, it tends to penetrate the fiber rather than bypass the fiber. Therefore, the polymer nanowires composite material can withstand a higher breakdown field than the polymer nanoparticle composite material. Moreover, considering the orientation of nws, It can also be seen from the simulation that vertically distributed nanowires can obstruct the external electric field more than parallel distributed nanowires. Therefore, nanocomposites with vertically arranged and randomly arranged nws in polymer matrix can successfully block the external electric field. On the other hand, 1D filled nanocomposites provide the highest polarizability, so the increase in dielectric constant is much larger than that of nanoparticles [6,27,28]. Therefore, according to the stimulation, the addition of dopamine modified BT nws will improved dielectric constant and breakdown voltage of composite effectively.

Weber distribution is used to characterize electrical breakdown performance of composite films, which are shown in Fig. 10. It can be seen from the figure, for the composite modified with dopamine, when the high dielectric constant filler is added to the polymer matrix, the total breakdown strength of the nanocomposite enhances and then reduces. The maximum breakdown voltage is 538 $kV·mm^{-1}$, which is comparable for pure ArPTU. This high breakdown voltage performance indicates that, since the amount of filler added is lower than its threshold volume fraction, composite film can successfully prevent conducting path from forming, such as electric field treeing, at high electrical field. Compared with pure polymer, the ordered and dense structure of Dapa@BT nanocomposite makes it highly insulating, which leads to a slightly increase in leakage current density in nanocomposite. During the solution casting of nanocomposite films, medium and high aspect ratio nanowires tend to be oriented in the in-plane direction, resulting in anisotropic polymer nanocomposite dielectrics. When an electric field is applied in an out-of-plane direction, these nanowires will cause the magnetic susceptibility anisotropy of the nanocomposite film, which leads to a decrease in the electric field concentration in the polymer matrix. In addition, the oriented nanowires in the nanocomposite can inhibit the growth of electrical conducting path, such as electric field treeing, by establishing a twisted tree-like path and acting as a scattering center for the charge carriers in the nanocomposite [28].

4.3.3 D-E electric hysteresis loop

The Fig. 11 shows the D-E loops of nanocomposite films with different weight fractions of nanowires under a varying electric field of 100 *Hz* at room temperature. It can be observed that the electrical displacement of the nanocomposite increases with the volume fraction of the nanofiller. This can be attributed to the higher dielectric constant of the BT nws. When the content of BT nws is 10 *wt.%* in terms of volume fraction, the electrical displacement of the nanocomposite shows the most significant enhancement. At the same time, the composite film exhibits a wider D-E loop, which deviates from the linear relationship between the electric displacement of the linear dielectric and the electric field. This phenomenon should be attributed to conductivity and dielectric loss, which further reduces the energy storage density of the nanocomposite. So, proper addition of BT nws would result in less hysteresis in composite film, achieving high dielectric constant and high energy storage efficiency accordingly.

4.3.4 Energy density and efficiency

Fig. 12 shows the energy storage density (Fig. 12(a).) and charge-discharge efficiency (Fig. 12(b).) of composite films. It has been found that an 7.5 J/cc^{-1} energy storage density is achieved, this is a comparably high energy storage density based on HDMLP and their composites. Furthermore, at a load of 3 *wt.%*, the discharge efficiency more than 90 % was achieved at 250 MV/m^{-1}. This could produce high energy density polymer dielectrics with high efficiency for practical capacitor applications. The efficiency of nanocomposites gradually decreases with the increase of nanowire load due to the increased loading of Dopa@BT nws, which results in increased hysteresis in composite. In conclusion, by combination of high dielectric constants BT nws with linear polymer dielectric ArPTU, a high performance composite dielectrics is constructed for practical high energy storage density capacitor applications.

5. Summary

High energy storage density and efficiency is achieved in composite dielectrics by compositing of HDMLP polymer with modified BT nws. The 1 D high-*k* filler with high aspect ratio has a large dipole moment, which shows an efficient increase in the dielectric constant of the nanocomposite. More importantly, the high aspect ratio of the one-dimensional high-*k* filler allows to achieve the ideal dielectric anisotropy in the nanocomposite by adjusting the spatial arrangement of the nanocomposite in the polymer matrix. Compared with the original polymer matrix, the modified BT nws incorporated composite films showed improved dielectric constant greatly, while the dielectric loss remains similar to that of pure ArPTU. In addition, the proposed nanocomposite material has demonstrated a significant increase in electrical displacement and energy density under high electric fields, and high discharge energy density was achieved. This work provides insights into constructing novel nanocomposite of polymer dielectrics with high energy storage density and efficiency for practical applications.

Declarations

Declaration of competing interest

The authors declare that they have no known competing financial interests or personal relationships that could have appeared to influence the work reported in this paper.

Acknowledgments

The work was supported by the National Natural Science Foundation of China (NSFC) (Grant Nos. 61774030 & 61971112); Natural Science Foundation of Chongqing(cstc2019jcyj-msxmX0824); Chongqing Postdoctoral Science Special Foundation (No. Xm2017051); Scientific Research Fund of Chongqing Municipal Education Commission (No. KJQN201901304); Foundation for High-level Talents of Chongqing University of Art and Sciences (No. R2016DQ11).

References

1. X. Zhang, B.-W. Li, L. Dong, H. Liu, W. Chen, Y. Shen, C.-W. Nan , Advanced Materials Interfaces, 5 (2018).
2. S. Wu, W. Li, M. Lin, Q. Burlingame, Q. Chen, A. Payzant, K. Xiao, Q.M. Zhang, Adv Mater, 25 (2013) 1734-1738.
3. S. Wu, Q. Burlingame, Z.-X. Cheng, M. Lin, Q.M , Journal of Electronic Materials, 43 (2014) 4548-4551.
4. W. Li, L. Jiang, X. Zhang, Y. Shen, C.W. Nan, J. Mater. Chem. A, 2 (2014) 15803-15807.
5. Q. Burlingame, S. Wu, M. Lin, Q.M. Zhang, Advanced Energy Materials, 3 (2013) 1051-1055.
6. X. Huang, B. Sun, Y. Zhu, S. Li, P. Jiang, Progress in Materials Science, 100 (2019) 187-225.
7. H. Luo, X. Zhou, C. Ellingford, Y. Zhang, S. Chen, K. Zhou, D. Zhang, C.R. Bowen, C. Wan, 48 (2019) 4424-4465.
8. H. Zhu, Z. Liu, F. Wang , Journal of Materials Science, 52 (2017) 5048-5059.
9. R. Ma, V. Sharma, A.F. Baldwin, M. Tefferi, I. Offenbach, M. Cakmak, R. Weiss, Y. Cao, R. Ramprasad, G.A. Sotzing, Journal of Materials Chemistry A, 3 (2015) 14845-14852.
10. T. Tian, R. Hu, B.Z. Tang, J Am Chem Soc, 140 (2018) 6156-6163.
11. C. Li, L. Shi, W. Yang, Y. Zhou, X. Li, C. Zhang, Y. Yang, Nanoscale Res Lett, 15 (2020) 36.
12. H. Tang, Y. Lin, H.A. Sodano, Advanced Energy Materials, 3 (2013) 451-456.
13. H. Zhang, Y. Zhu, Z. Li, P. Fan, W. Ma, B. Xie, Journal of Alloys and Compounds, 744 (2018) 116-123.
14. H. Tang, Z. Zhou, H.A. Sodano, ACS Appl Mater Interfaces, 6 (2014) 5450-5455.
15. Jiang C, Kiyofumi K, Wang Y,Koumoto K, Journal Article,7 (2007) 2713–2715.
16. N. Bao, L. Shen, A. Gupta, A. Tatarenko, G. Srinivasan, K. Yanagisawa, Applied Physics Letters, 94 (2009).
17. G. Wang, X. Huang, P. Jiang, ACS Appl Mater Interfaces, 7 (2015) 18017-18027.
18. H. Hu, F. Zhang, S. Lim, P. Blanloeuil, Y. Yao, Y. Guo, C.H. Wang, Composites Part B: Engineering, 178 (2019).
19. Y. Song, Y. Shen, H. Liu, Y. Lin, M. Li, C.-W. Nan, Journal of Materials Chemistry, 22 (2012).

20. Y. Song, Y. Shen, H. Liu, Y. Lin, M. Li, C.-W. Nan, Journal of Materials Chemistry, 22 (2012).
21. S.-O. Kang, H.-S. Jang, K.-B. Kim, B.H. Park, M.-J. Jung, Y.-I. Kim, Materials Research Bulletin, 43 (2008) 996-1003.
22. M. Teresa Buscaglia, C. Harnagea, M. Dapiaggi, V. Buscaglia, A. Pignolet, P. Nanni, Chemistry of Materials, 21 (2009) 5058-5065.
23. L. Xie, X. Huang, C. Wu, P. Jiang, Journal of Materials Chemistry, 21 (2011).
24. S. Liu, J. Zhai, Journal of Materials Chemistry A, 3 (2015) 1511-1517.
25. Y. Yang, J. He, Q. Li, L. Gao, J. Hu, R. Zeng, J. Qin, S.X. Wang, Q. Wang, Nat Nanotechnol, 14 (2019) 151-155.
26. Prateek, V.K. Thakur, R.K. Gupta , Chemical Reviews, 116 (2016) 4260-4317.
27. Z.H. Shen, J.J. Wang, Y. Lin, C.W. Nan, L.Q. Chen, Y. Shen, Adv Mater, 30 (2018).
28. Y. Hao, X. Wang, K. Bi, J. Zhang, Y. Huang, L. Wu, P. Zhao, K. Xu, M. Lei, L. Li, Nano Energy, 31 (2017) 49-56.

Figures

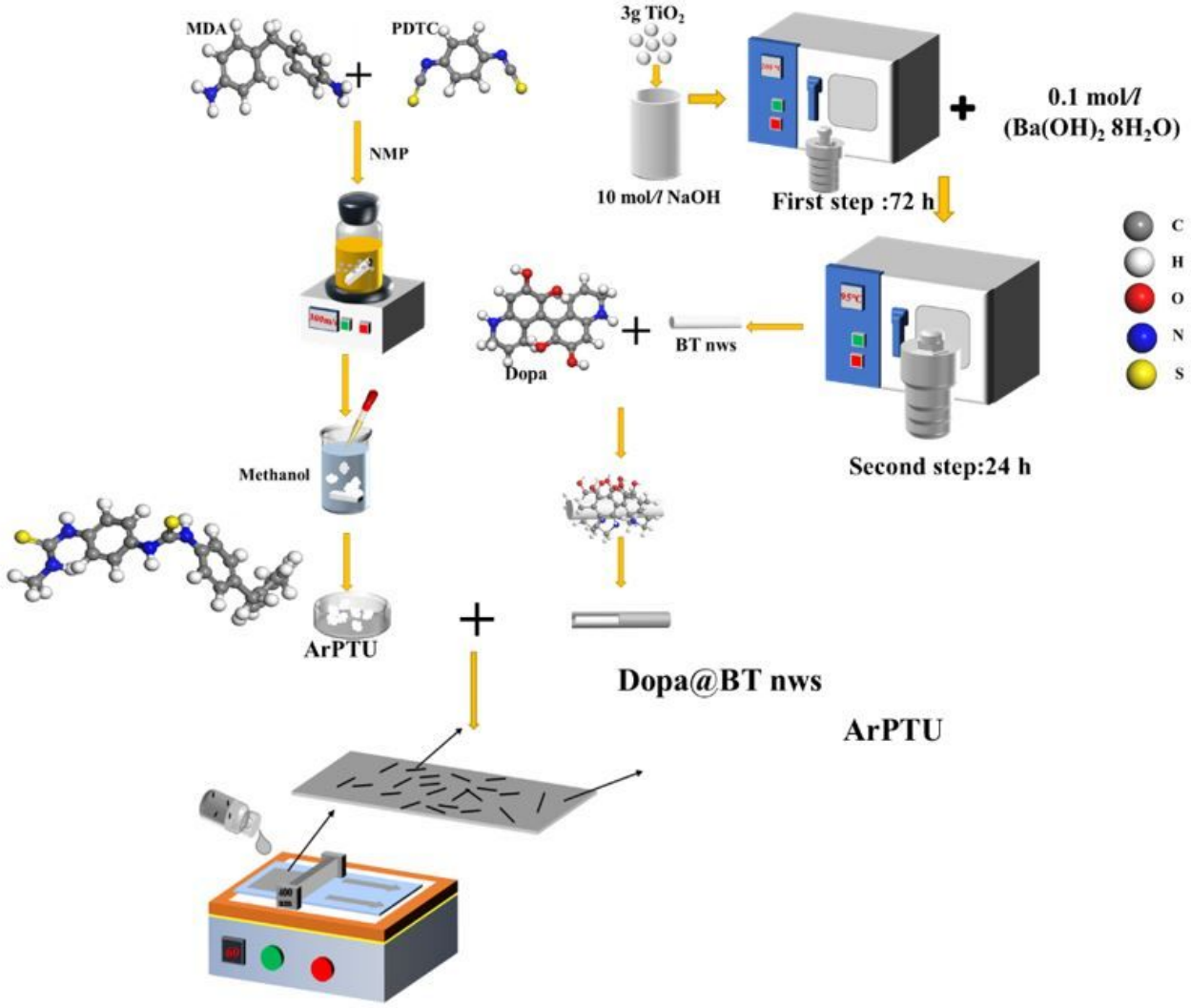

Figure 1

The schematic illustration of preparation process of dielectric composite film

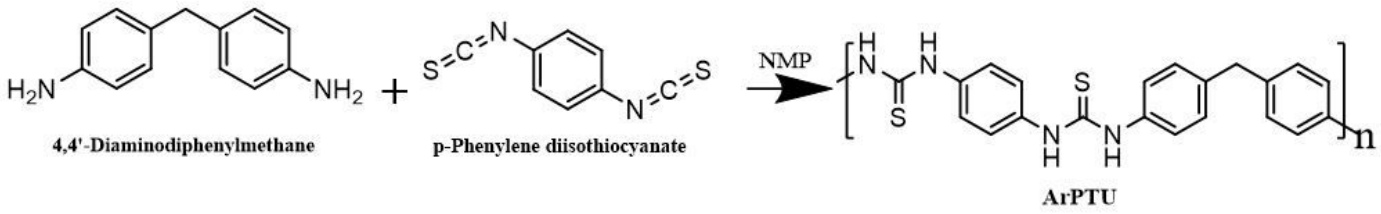

Figure 2

Schematic of synthesis of ArPTU via polycondensation of MDA and PDTC

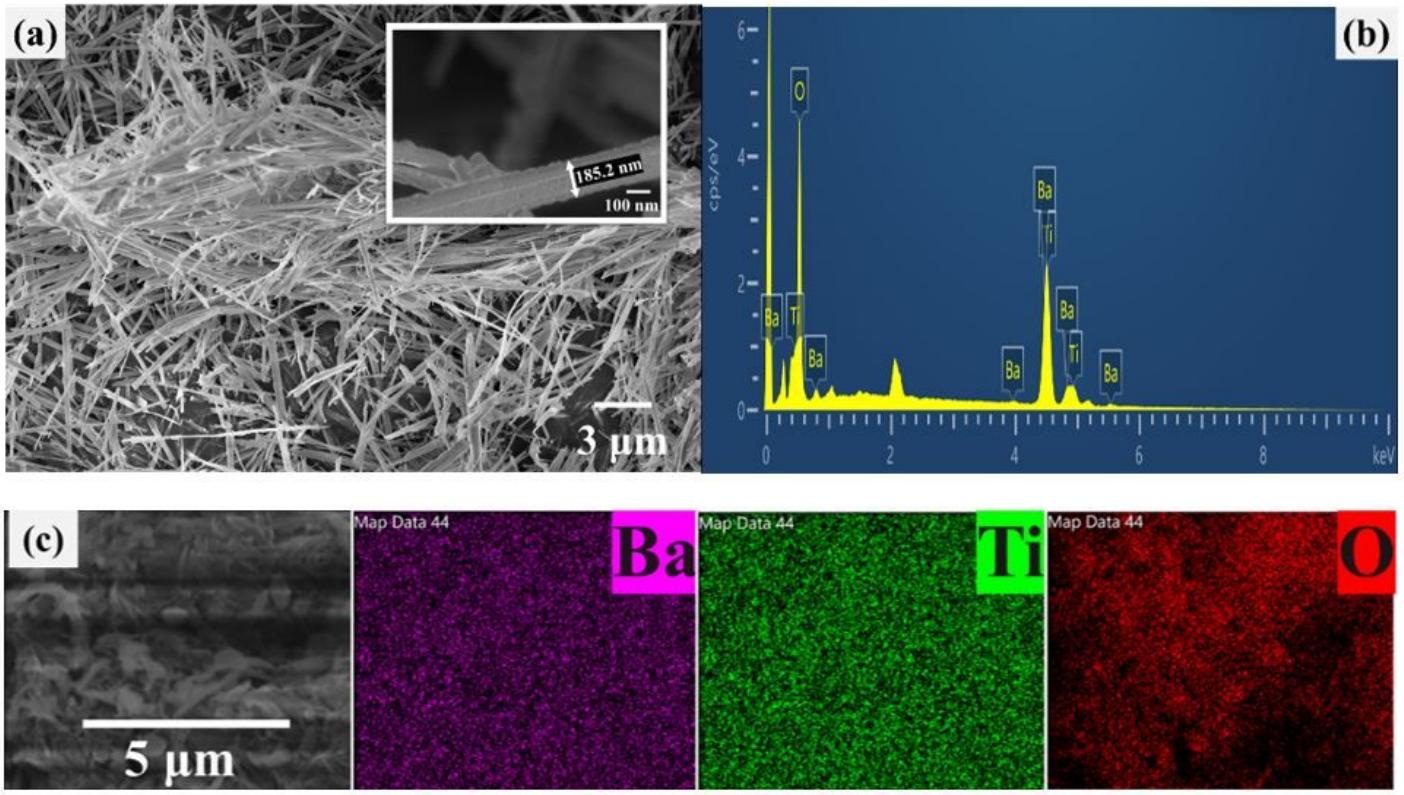

Figure 3

Morphology analysis of BT nws. (a) SEM image of BT nws. (b,c) Elemental analysis of BT nws.

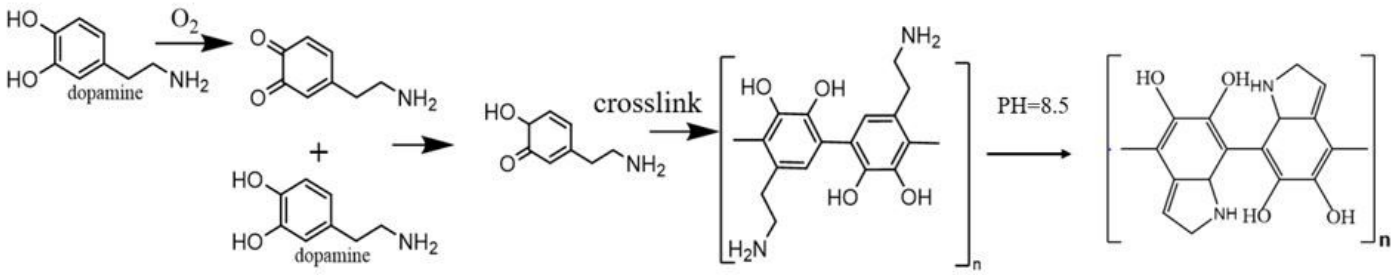

Figure 4

Self-polymerization of Dopa

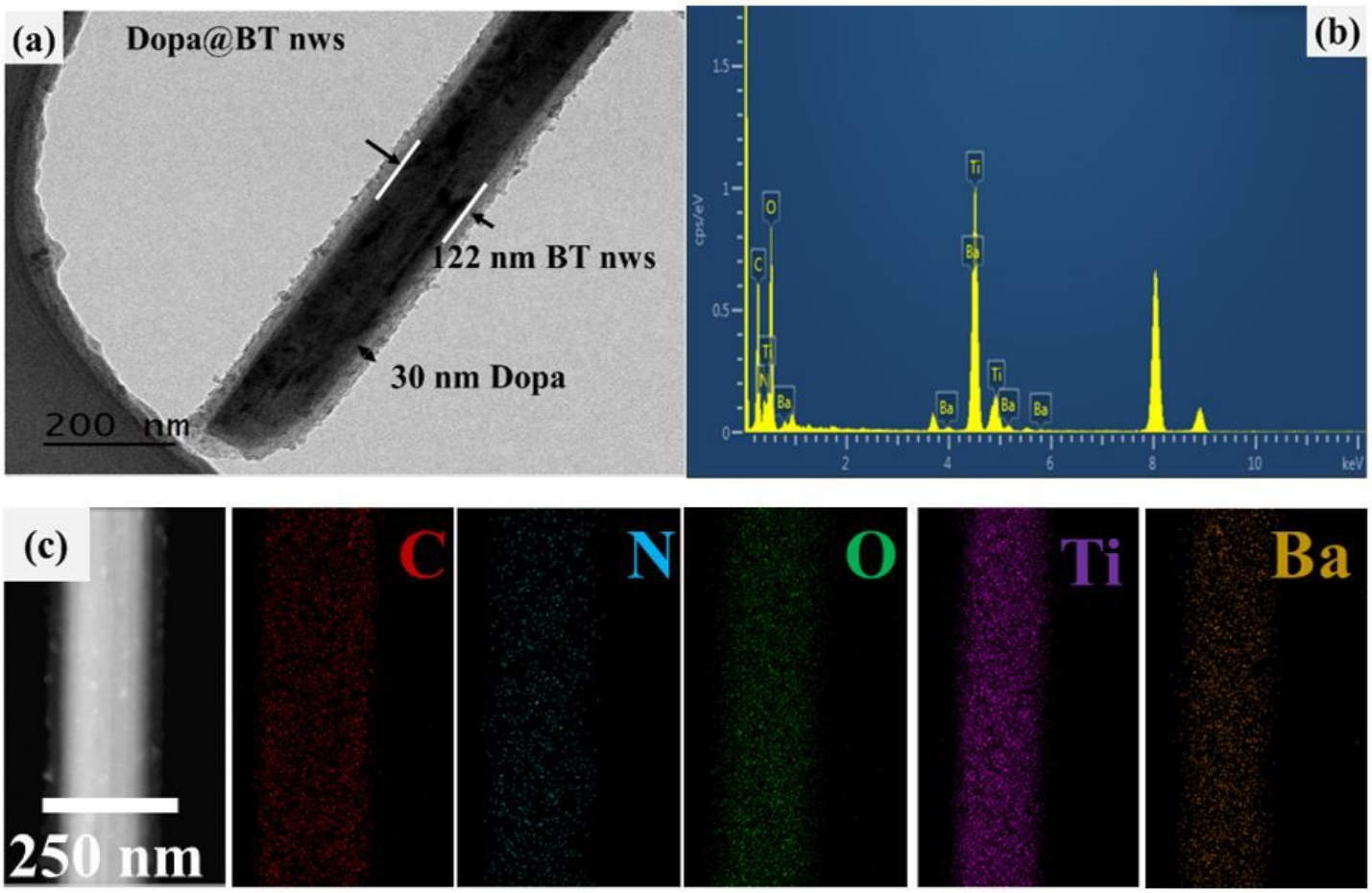

Figure 5

Morphology analysis of Dopa@BT nws. (a) TEM image of Dopa@BT nws. (b,c) Elemental analysis of Dopa@BT nws.

Figure 6

Contact angle of BT nws and Dopa@BT nws. (a) Contact angle of BT nws. (b) Contact angle of Dopa@BT nws

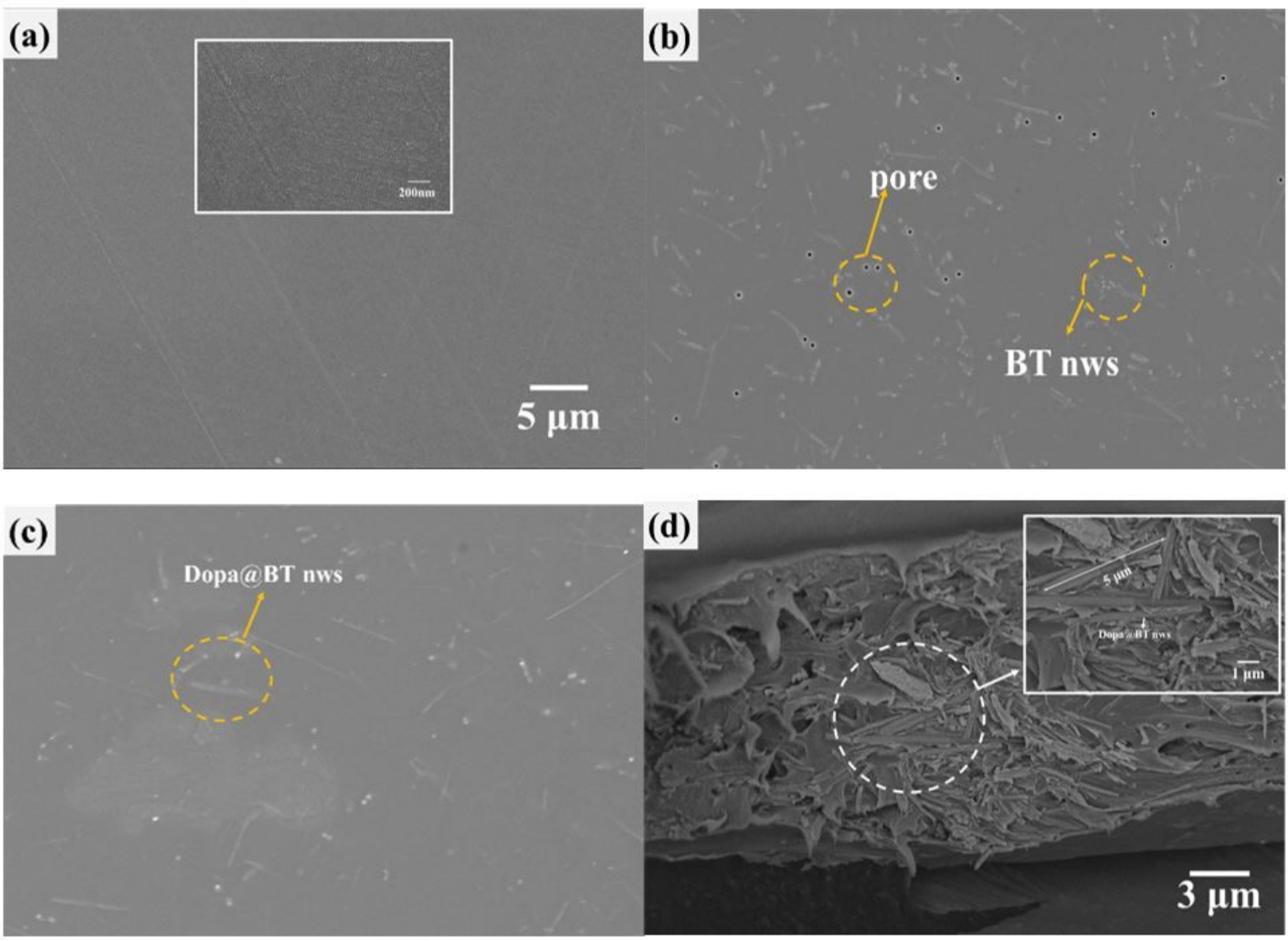

Figure 7

Micro-topography of ArPTU and composite film. (a) SEM images of pure ArPTU. (b) SEM images of 10 wt.% BT nws composite film. (c) SEM of 10 wt.% Dopa@BT nws composite film. (d) Cross-sectional SEM image of 10 wt.% Dopa@BT nws composite film.

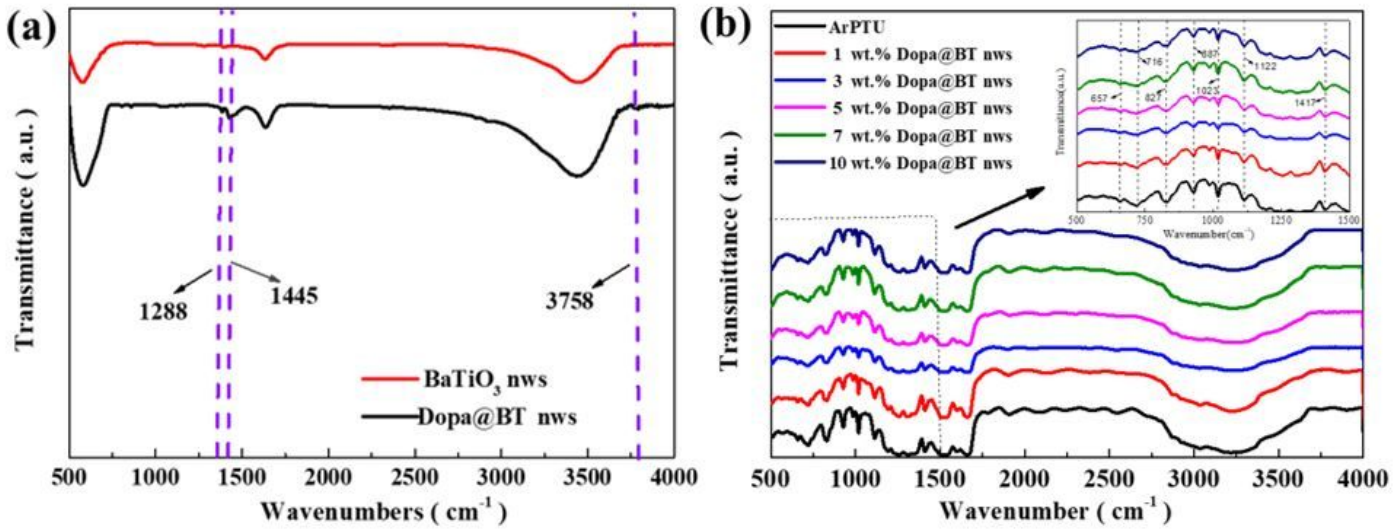

Figure 8

FTIR spectra of BT,Dopa@BT nws and composite film.(a) FTIR spectra of BT and Dopa@BT nws.(b) FTIR spectrum of composite film

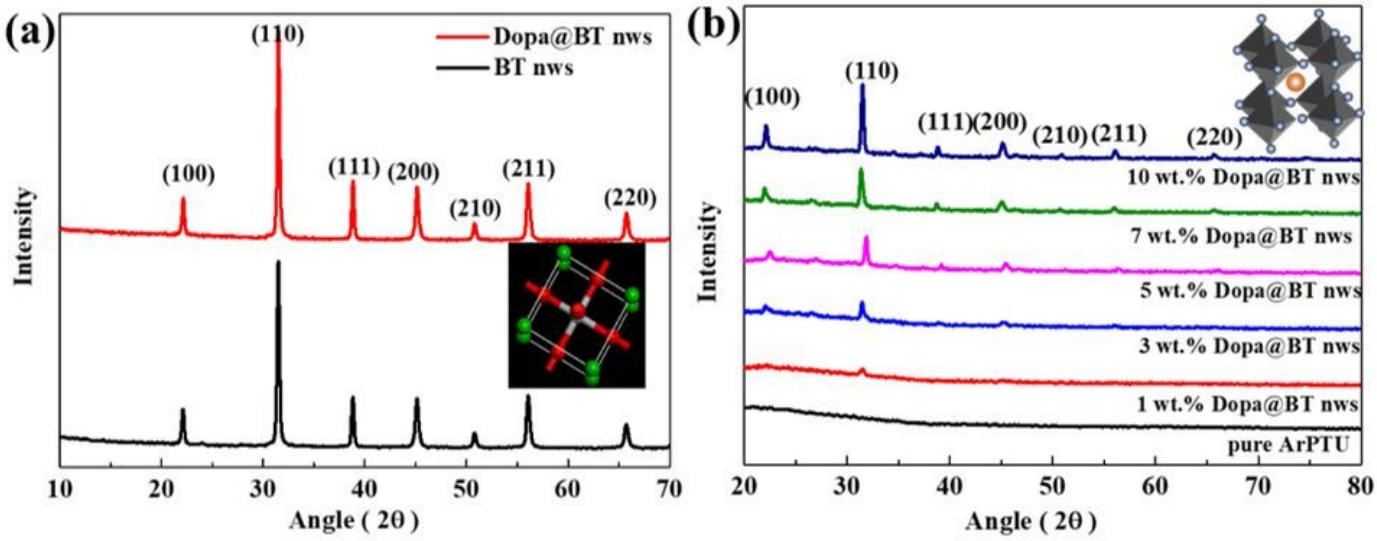

Figure 9

XRD of BT, Dopa@BT nws and composite film. (a) XRD of BT and Dopa@BT nws. (b) XRD of composite film

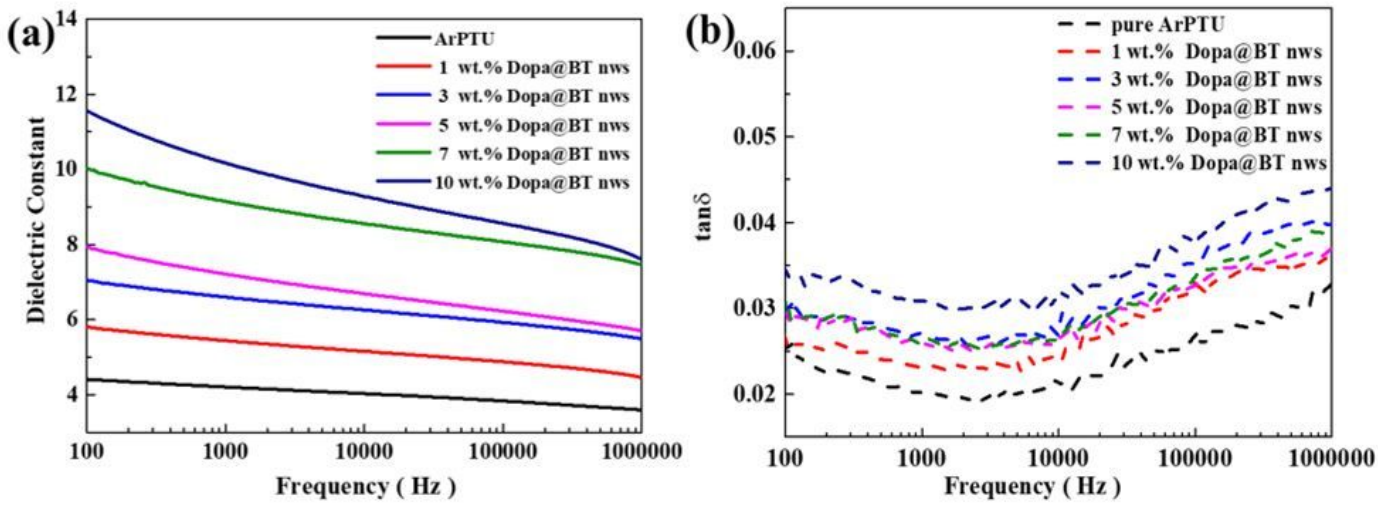

Figure 10

Dielectric properties graph of composite film.(a) Dielectric constant of composite film.(b) Dielectric loss of composite film

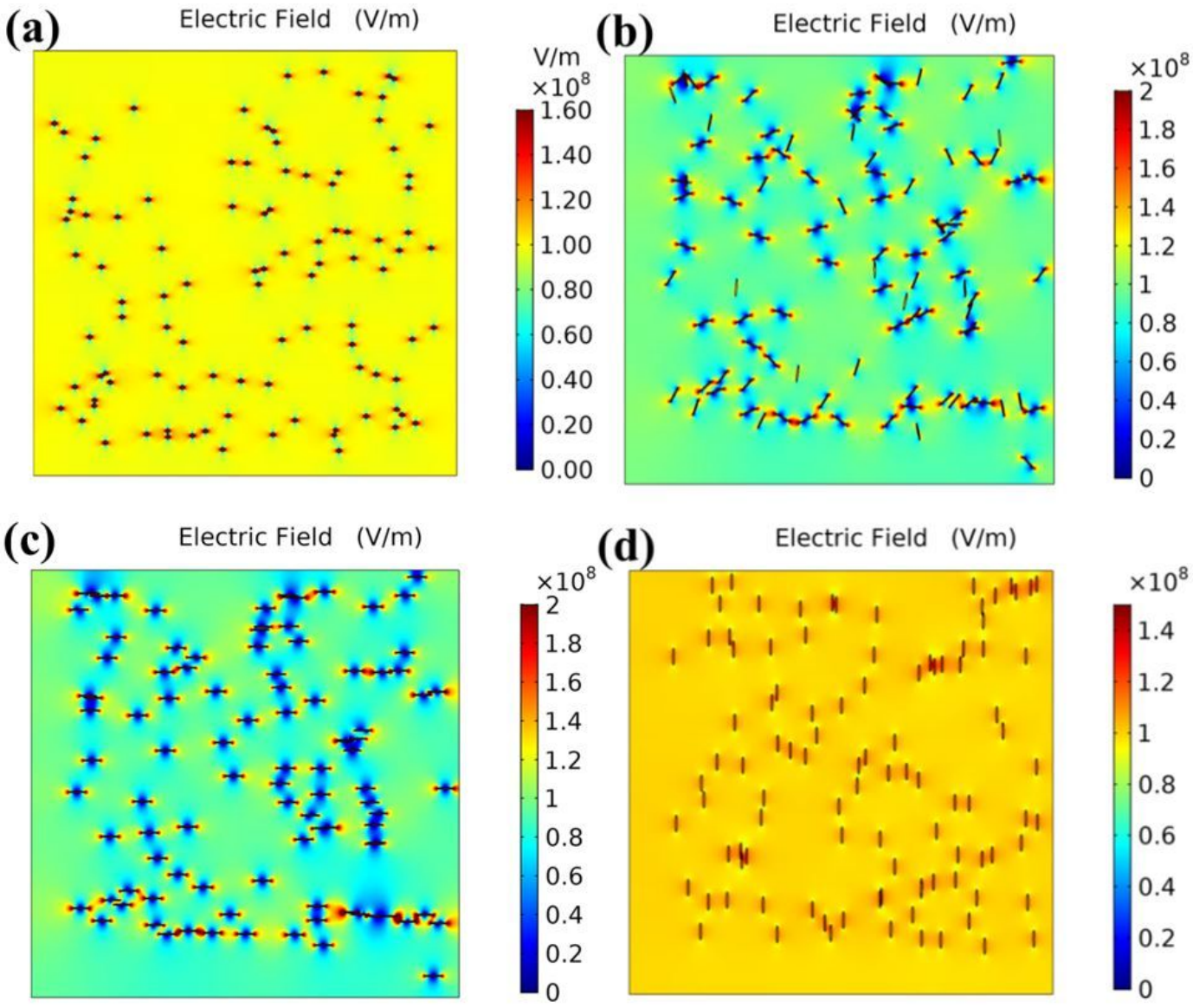

Figure 11

Electric field distribution of composite films incorporated with nanoparticles and nanowires.(a) Random distribution of nanoparticles.(b) Random distribution of nanowires. (c) Vertical electric field distribution of nanowires.(d) Parallel electric field distribution of nanowires

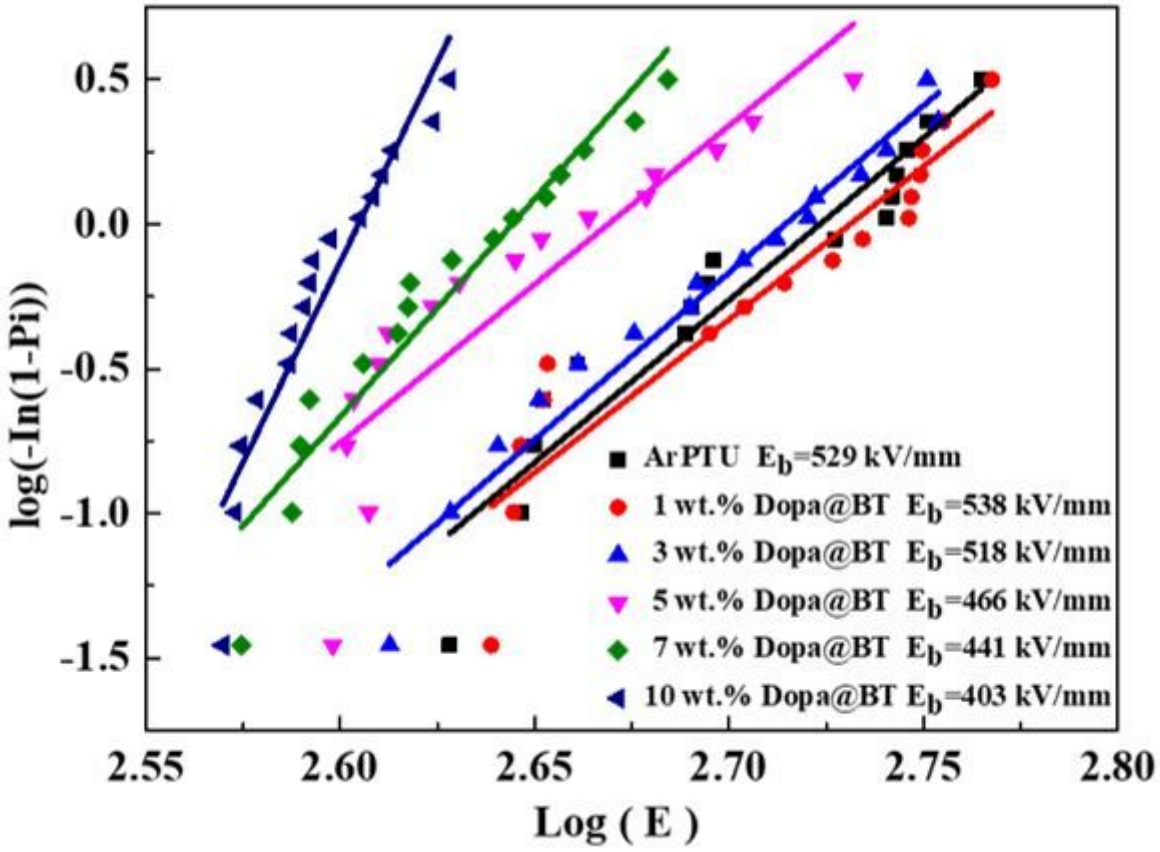

Figure 12

Weber distribution of composite film

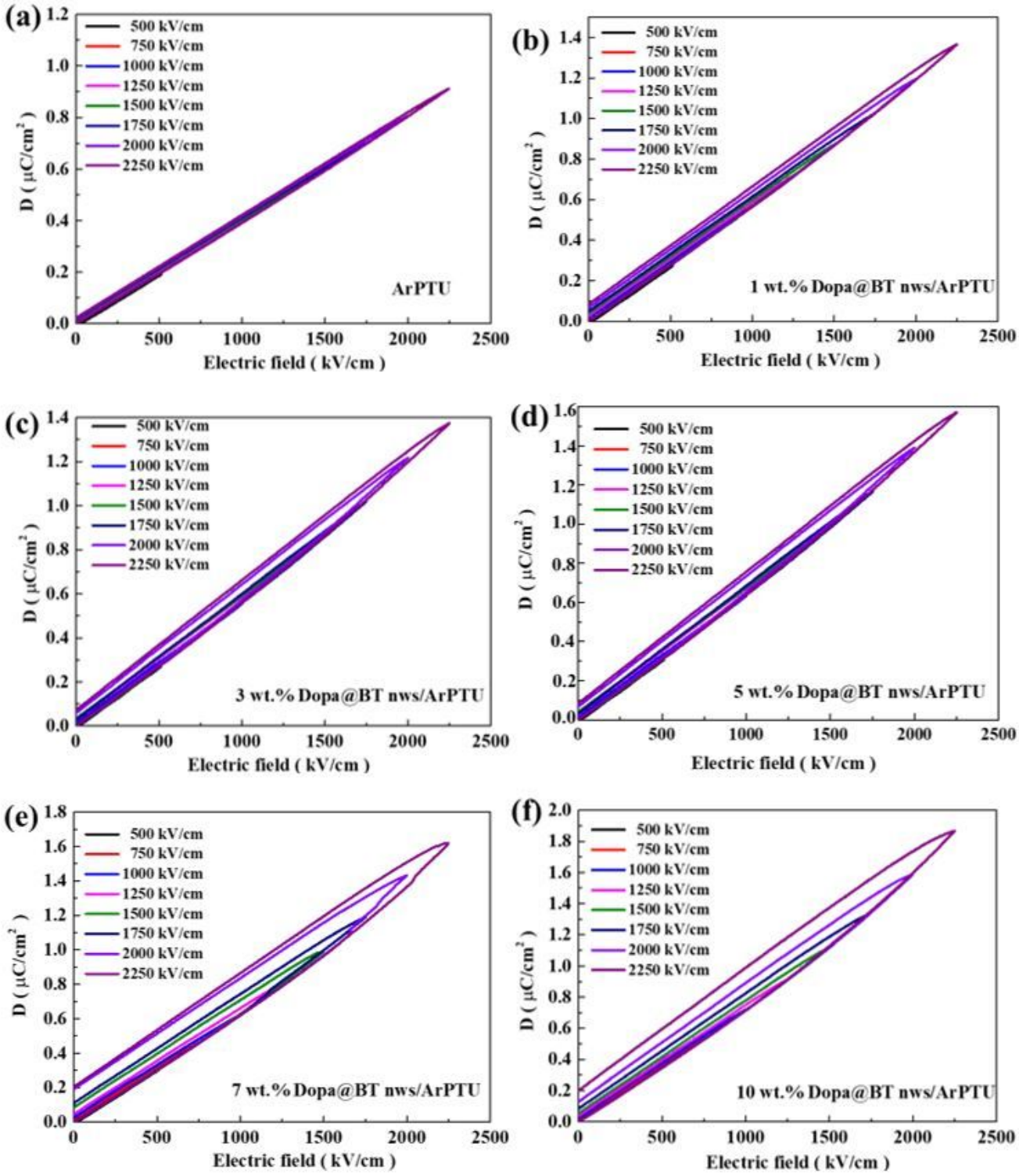

Figure 13

D-E curves of pure ArPTU and Dopa@BT nws and composite films with different mass fractions Dopa@BT nws.(a) pure ArPTU.(b) 1 wt.% .(c) 3 wt.% .(d) 5 wt.% .(e) 7 wt.% .(f) 10 wt.% .

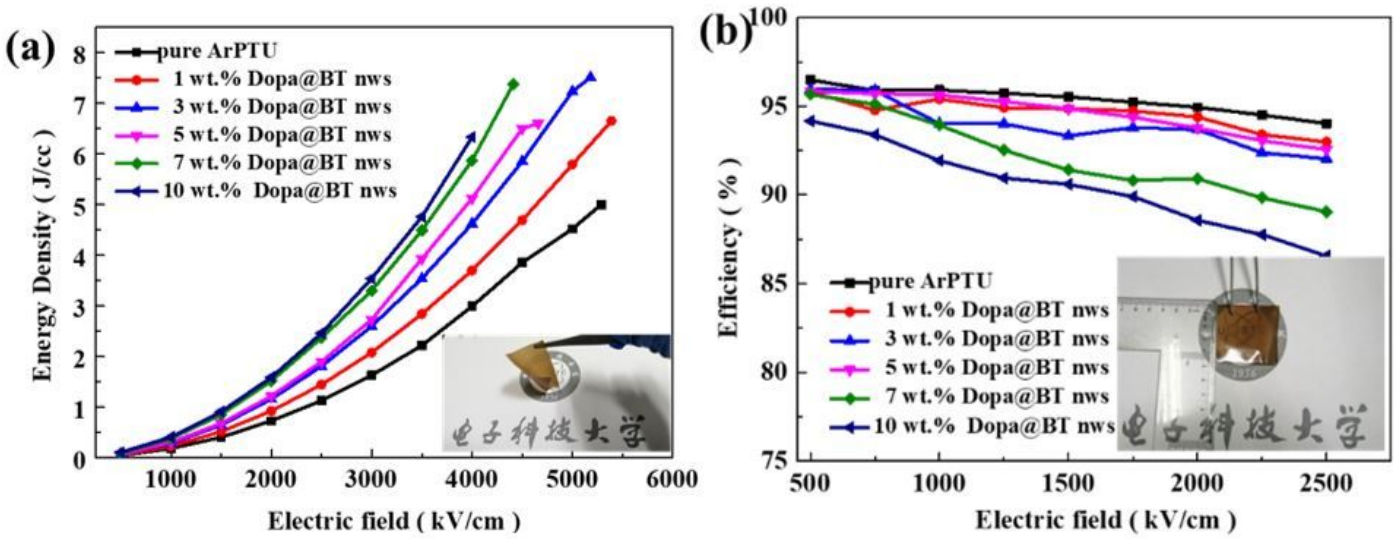

Figure 14

Energy density and charge-discharge efficiency diagram of ArPTU-based nanocomposites with different electric field. (a) Energy density. (b) charge-discharge efficiency